Nanoscale

Accepted Manuscript

This is an *Accepted Manuscript*, which has been through the RSC Publishing peer review process and has been accepted for publication.

Accepted Manuscripts are published online shortly after acceptance, which is prior to technical editing, formatting and proof reading. This free service from RSC Publishing allows authors to make their results available to the community, in citable form, before publication of the edited article. This *Accepted Manuscript* will be replaced by the edited and formatted *Advance Article* as soon as this is available.

To cite this manuscript please use its permanent Digital Object Identifier (DOI®), which is identical for all formats of publication.

More information about *Accepted Manuscripts* can be found in the **Information for Authors**.

Please note that technical editing may introduce minor changes to the text and/or graphics contained in the manuscript submitted by the author(s) which may alter content, and that the standard **Terms & Conditions** and the **ethical guidelines** that apply to the journal are still applicable. In no event shall the RSC be held responsible for any errors or omissions in these *Accepted Manuscript* manuscripts or any consequences arising from the use of any information contained in them.

Cite this: DOI: 10.1039/c0xx00000x

www.rsc.org/xxxxxx

ARTICLE TYPE

Multi-functional $NaErF_4$:Yb nanorods: enhanced red upconversion emission, *in vitro* cell, *in vivo* X-ray, and T_2-weighted magnetic resonance imaging

Haibo Wang,[a,b] Wei Lu,[c] Tianmei Zeng,[a] Zhigao Yi, [a,b] Ling Rao, [a,b] Hongrong Liu[a] and Songjun Zeng[*a]

Received (in XXX, XXX) Xth XXXXXXXXX 20XX, Accepted Xth XXXXXXXXX 20XX
DOI: 10.1039/b000000x

In this paper, multi-functional hexagonal phase $NaErF_4$:Yb nanorods were synthesized by a facile hydrothermal method. The upconversion luminescence (UCL) intensity and red to green ratio of the multi-functional $NaErF_4$ nanorods can be improved by Yb^{3+} doping. More importantly, owing to the decreased distant of Er and Yb, the significant enhancement of red UCL can be obtained, which is different with the usual green UCL of Yb/Er doped $NaYF_4$ host. In addition, the intensity of UCL is strongest when the Yb^{3+}-doped concentration reached 30%. The *in vitro* cell imaging and localized UCL spectra taken from HeLa cells revealed that these $NaErF_4$: 30% Yb^{3+} nanorods are ideal nanoprobes with absent autofluorescence for optical bioimaging. Moreover, these nanorods possess large X-ray absorption ions (Er^{3+} and doped Yb^{3+}), and were successfully used as contrast agent for *in vivo* X-ray bioimaging for the first time. In addition to the excellent UCL and X-ray absorption properties, these nanorods present large paramagnetic property and can be used as T_2-weighted magnetic resonance imaging (MRI) agent. Therefore, these enhanced red UCL $NaErF_4$ nanocrystals with excellent paramagnetic property and X-ray absorption properties can be used as promising multi-modal nanoprobes for optical bioimaging, MRI, computed X-ray tomography (CT), and may have potential applications in bioseparation.

1. Introduction

In recent years, lanthanide (Ln) doped upconversion (UC) nanocrystals have stimulated considerable interest in bioimaging. Compared to conventional semiconductor quantum dots and organic dyes, Ln^{3+}-doped UC nanocrystals are superior in terms of deep penetration, low radiation damage, and weak auto-fluorescence, owing to undergo a process known as UC of converting low energy irradiation (typically 980 nm) to high energy emissions.[1-30] In addition, UC emissions have been studied in various host materials such as fluorides, oxides, vanadates, and chlorides. Among of them, sodium rare earth fluorides ($NaREF_4$) have been considered as excellent hosts owing to the relative low phonon energy leading to low non-radiative relaxation probability.[31] Most of the reports have focused on the Y-based host ($NaYF_4$:Yb/Er), which is also considered as a most efficient host. However, the Yb/Er co-doped $NaYF_4$ host usually present intense green emission (<600 nm). While, the intense red UC emission centered at about 660 nm is more beneficial for optical bioimaging owing to the low tissue absorption. Therefore, it is of significant importance to achieve intense red UC emission for optical bioimaging application. As a potential host material, $NaErF_4$ nanocrystals possess unique red UCL,[32] owing to the decreased distance of Er^{3+}, which is different with the well-established $NaYF_4$ host usually presenting green UCL. However, it is still a great challenge to improve the UC intensity of $NaErF_4$ owing to the low absorption efficiency of 980 nm excitation light of Er^{3+}. According to the previous reports,[9,33] doping Yb^{3+} can remarkably improve the UCL property by efficient energy transfer between Yb^{3+} and Er^{3+} and larger absorption coefficient for 980 nm light of Yb^{3+}.

On the other hand, although fluorescent imaging can provide high sensitivity and spatial resolution, it suffers from poor-tissue penetration, limiting its use for deep-tissue imaging which can be solved by MRI and X-ray imaging.[19,34-36] Therefore, developing an approach to combine the advantage of X-ray imaging, MRI, and fluorescent imaging will be of great importance. Compared with the Y-based host, the Er-based host can not only have unique UCL property but also possess large intrinsic magnetic moment (9.59 μ_B)[37] and K-edge energy (57.49 keV)[38,39], which make these Er-based materials promising agents for MRI and X-ray imaging.[32] To the best of our knowledge, multi-functional $NaErF_4$:Yb probes with enhanced red UC emission for *in vitro* cell, T_2-weighted magnetic resonance imaging and *in vivo* X-ray imaging have not been exploited yet.

In this paper, multi-functional $NaErF_4$:Yb nanocrystals were synthesized by a simple hydrothermal method using oleic acid (OA) as capping agent. Moreover, the UCL properties of the $NaErF_4$ nanocrystals doped with different Yb^{3+} contents were investigated under 980 nm laser diode (LD) excitation. The *in vitro* cell imaging was demonstrated for the first time by using the HCl treated $NaErF_4$: 30% Yb^{3+} nanocrystals. Moreover, owing to the large magnetic moment, the T_2-weighted MRI was performed. More importantly, these nanocrystals were also

successfully used as contrast agent for *in vivo* X-ray imaging for the first time.

2. Experimental

$Er(NO_3)_3·6H_2O$ (99.99%) and $Yb(NO_3)_3·5H_2O$ (99.99%) were purchased from Sinopharm Chemical Reagent Co., Ltd (China). All other chemicals are analytical grade and used directly without further purification.

2.1. Synthesis of Yb^{3+}-doped $NaErF_4$ nanocrystals

$NaErF_4$: X% Yb^{3+} (X=5, 10, 30, and 40) nanocrystals were synthesized by a hydrothermal method as previously reported.[40,41] The synthesis of Yb^{3+}-doped $NaErF_4$ nanocrystals was conducted following a typical protocol, 10 mL of ethanol was added into 2 mL of an aqueous solution containing 1.2 g of NaOH under stirring to form a homogeneous solution. Following, 20 mL of OA was added to the above solution to form a sodium-OA complex. Subsequently, 1 mmol of $RE(NO_3)_3$ (RE=Er, Yb with designed molar ratios) and 8 mL of NaF (1.0 M) solutions were added under vigorously stirring for 10-20 min. The obtained solution was then transferred into a 50 mL stainless Teflon-lined autoclave, which was reacted at 190 ℃ for 12 h. The system was cooled to room temperature naturally. The resulting precipitates were separated by centrifugation, washed three times with ethanol and de-ionized water to remove OA and other residual solvents, and then dried at 60 ℃ for 10 h.

2.2. Synthesis of hydrophilic ligand-free $NaErF_4$: 30% Yb nanorods

To convert the hydrophobic OA-coated $NaErF_4$: 30% Yb nanorods to the hydrophilic ligand-free nanorods, a HCl treated method developed by Capobianco's group was adopted.[42] First, 100 mg of OA-coated $NaErF_4$: 30% Yb nanorods were dispersed in 10 mL of aqueous solution. Then, adding a solution of HCl (0.1 M) to maintain the pH at 4 under vigorously stirring. After stirring for 2 h, the solution was mixed with diethyl ether to remove the OA by extraction with diethyl ether three times and the combined ether layers were re-extracted with water. The ligand-free nanorods in the water dispersible fraction were separated by centrifugation after precipitated with acetone. Finally, the hydrophilic ligand-free $NaErF_4$: 30% Yb nanorods were dispersed in water for the later bioimaging assay.

2.3. Characterizations.

The X-ray powder diffraction (XRD) analysis of the as-prepared samples was performed using a Rigaku D/max 2500/PC X-ray diffractometer at 40 kV and 250 mA with Cu Kα radiation (λ=1.5406 Å). The size and morphology of the samples were characterized by transmission electron microscopy (TEM, JEOL-2100F) equipped with an energy-dispersive X-ray spectrometer (EDS). The UC emission spectra were obtained by a spectrophotometer (R500) equipped with an excitation source (980 nm LD). The digital photographs of the as-prepared samples were taken by a commercial digital camera (Canon 650D).

2.4. Cell culture and *in vitro* upconversion fluorescent imaging

HeLa (human cervical carcinoma cell line) cells were obtained from the Institute of Biochemistry and Cell Biology, SIBS, CAS (China), the cells were incubated in Dulbecco's Modified Eagle's Medium (DMEM) supplemented with 10% fetal bovine serum and 1% penicillin and streptomycin at 37 ℃ and 5% CO_2. UC fluorescent imaging of HeLa Cells incubated with ligand-free $NaErF_4$: 30% Yb^{3+} (100 μg/mL) for 4 h was performed on a commercial con-focal laser scanning microscope (ZEISS LSM-710 NLO). The luminescent signals were detected in the red UC channel (600-700 nm).

2.5. Phantom magnetic resonance imaging

To demonstrate the T_2-weighted MRI, various molar concentrations (0, 0.2, 0.4, 0.6, and 0.8 mM) of ligand-free $NaErF_4$: 30% Yb^{3+} nanorods were tested under a 4.7 T magnetic resonance image scanner (Bruker Biospec). The parameters of T_2-weighted MRI were used as follows: TR/TE=3000/30 ms, 128*128 matrices, and a slice thickness of 1.0 mm.

2.6. *In vivo* X-ray imaging

To demonstrate the ability of X-ray imaging, a nude mouse was first anesthetized. And then 200 μL of the ligand-free $NaErF_4$: 30% Yb^{3+} nanorods aqueous solution with concentration of 3 mg/mL was subcutaneously injected into the mouse. After injection, *in vivo* X-ray imaging was tested by a Carestream *In-Vivo* FX PRO imaging system under the operating voltage of 35 kVp. All animal procedures comply with the institutional animal use and care regulations.

3. Results and discussion

3.1. Structure control

Figure 1 shows the XRD results of $NaErF_4$: X% Yb (5, 10, 30, and 40) nanorods. As demonstrated in Figure 1a-c, all of the diffraction peaks of $NaErF_4$: X% Yb (5, 10, and 30) nanorods are matched well with the standard hexagonal phase $NaErF_4$ (JCPDS card no. 27-0689). No other impurity diffraction peak was observed, indicating that pure hexagonal phase nanorods with good crystallinity were synthesized and a homogenous Er-Yb solid solution structure was formed. Moreover, when the Yb^{3+} content reaches 40% (Figure 1d), the as-synthesized nanocrystals consist of two phases, i.e., the cubic phase (marked by red asterisk) and the hexagonal phase. It's noted that the diffraction peak marked with blue symbol (v) is attributed to the residual NaF. The diffraction peaks of cubic phase (Figure 1d) are broader than hexagonal phase nanorods, owing to the formation of small sized cubic phase particles, which is further verified by later TEM results. Based on the above analysis, the crystal phase of $NaErF_4$:Yb nanocrystals can be tuned by doping different Yb^{3+} content. The hexagonal phase $NaErF_4$:Yb nanocrystals can be obtained at lower Yb^{3+} doping content.

The morphology and structure of $NaErF_4$ nanocrystals doped with different contents of Yb^{3+} were further examined by TEM. As shown in Figure 2a (5% Yb) and 2b (10% Yb), the as-synthesized nanorods exhibit excellent monodispersity with the length of about 640 nm and diameter of about 75 nm. The inset of Figure 2a shows the corresponding high-resolution transmission electron microscopy (HRTEM) image of as individual nanorod. The distances between the parallel lattice planes are measured to be 3.62 Å and 5.16 Å, which are well coincident with the (001)

and (100) crystal planes of the hexagonal phase $NaErF_4$ structure (Figure 1a), respectively. With increasing the Yb^{3+} content to 30% (Figure 2c), the nanocrystals still maintain the rod-like structure with size of about 810 nm (length) and 115 nm (diameter). In addition, when the Yb^{3+} content reached 40% (Figure 2d), two distinct structures including small nanocubes (about 15 nm) and large nanorods were observed. The corresponding selected area electron diffraction (SAED) image of the nanocubes (the inset of Figure 2d) reveals that the nanoparticles have a face-centered cubic (FCC) phase structure, which is well consistent with the aforementioned XRD results. According to Liu's first principle calculations [8], $NaLnF_4$ host with smaller Ln^{3+} radius is more energetically stable than larger Ln^{3+} in cubic phase. Therefore, in our study, the crystal phase transformation (from hexagonal to cubic phase), is mainly ascribed to the substitution of Er^{3+} (radius = 1.144 Å) by the smaller Yb^{3+} (radius = 1.125 Å).[43] The elemental analysis of the $NaErF_4$: 30% Yb^{3+} nanorods performed by EDS reveals the presence of Na, Er, F and doped Yb.

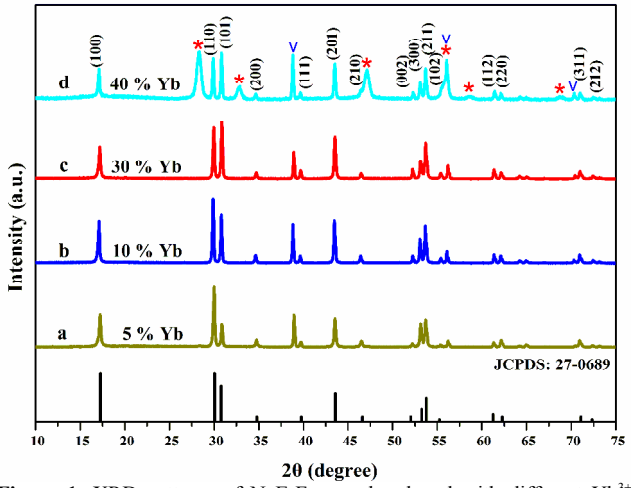

Figure 1. XRD patterns of $NaErF_4$ samples doped with different Yb^{3+} contents: (a) 5%, (b) 10%, (c) 30%, and (d) 40%. The diffraction peaks of the cubic phase are indicated by the red asterisk. The diffraction peak marked with blue symbol v, denotes the residual NaF structure.

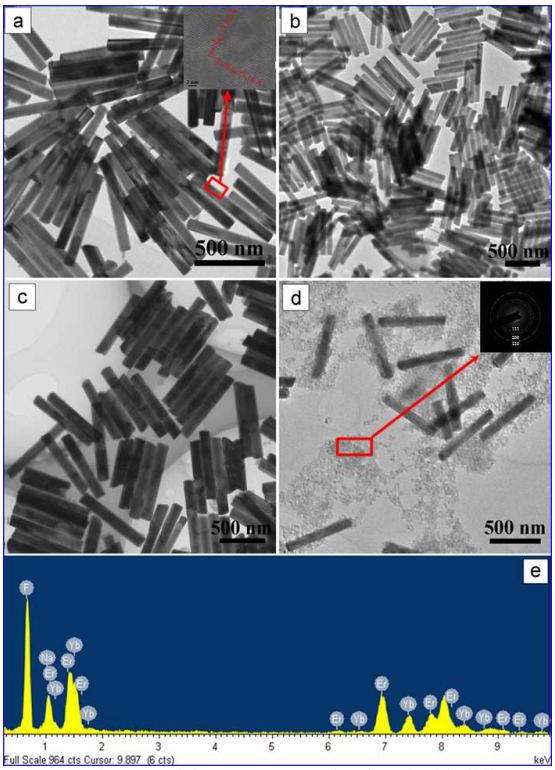

Figure 2. TEM images of the $NaErF_4$ samples doped with different contents of Yb^{3+} (a) 5%, (b) 10%, (c) 30%, (d) 40%. (e) EDS of the $NaErF_4$: 30% Yb^{3+} nanocrystals (mainly composed of Na, Er, Yb, and F elements). The inset of Figure 2a shows the corresponding HRTEM image. The inset of (d) shows the corresponding selected area electron diffraction pattern.

3.2. Enhanced UCL properties and dominant red UCL

To further study the influence of Yb^{3+} contents on UCL intensity, UC properties of $NaErF_4$: X% Yb^{3+} (X= 5, 10, 30, and 40) were studied. As shown in UCL spectra (Figure 3b), all samples exhibit superior red UC emission peaks centered at 664 nm and weaker green UCL around at 520 nm, 545 nm, assigned to the $^4F_{9/2} \rightarrow {}^4I_{15/2}$, $^2H_{11/2} \rightarrow {}^4I_{15/2}$, and $^4S_{3/2} \rightarrow {}^4I_{15/2}$ transitions of Er^{3+} (Figure 3a), respectively. The red to green intensity ratio (R/G) of various Yb^{3+} contents doped $NaErF_4$ nanocrystals are measured to 6.9 (5% Yb^{3+}), 13.8 (10% Yb^{3+}), 9 (30% Yb^{3+}), and 5.5 (40% Yb^{3+}), respectively. It should be noted that the R/G in the $NaErF_4$ host is significantly different from Yb/Er doped $NaYF_4$ host with R/G of 0.077.[44] The large R/G in $NaErF_4$ host make them present intense eye-visible red UCL, which is vividly verified in digital photographs (insets of Figure 3b). The dominant red UCL is mainly ascribed to the effective cross relaxation (CR) process ($^4F_{7/2} \rightarrow {}^4F_{9/2}$, $^4F_{9/2} \leftarrow {}^4I_{11/2}$) between the adjacent Er^{3+} ions owing to the small distance of Er^{3+} in $NaErF_4$ host. The short distance of Er^{3+} may increase the CR (Figure 3a) process, resulting in remarkable enhancement of the population in $^4F_{9/2}$ energy level of Er^{3+}.[32] It is generally believed that the absorbance and autofluorescence of tissue are minimum in red region (600-700 nm). Consequently, the dark red emission falls within the 'optical window' that could afford the deep tissue penetration in *in vivo* bioimaging. Therefore, compared with Yb/Er co-doped $NaYF_4$ nanocrystals with green UCL, Yb doped $NaErF_4$ host with strong red emission (664 nm) is more suitable for high contrast optical bioimaging owing to the lower tissue absorption.

In addition, with increasing the Yb^{3+} content, the UCL intensity was gradually increased. When the doped Yb^{3+} reached up to 30%, the sample presents the strongest UCL. However, while further increasing the doped Yb^{3+} content to 40%, the UCL intensity is dramatically decreased owing to the formation of new phase (cubic phase) with small size (about 15 nm). Smaller sized nanocrystals may increase surface quenching sites and consequently suppress UC process by enhanced non-radiative energy transfer processes.[8] Two possible reasons are mainly responsible for the initial increased UCL: First, with doping Yb^{3+} into the $NaErF_4$ host, the inter-atomic distance of Yb-Er will be decreased and the back-energy-transfer from Yb^{3+} to Er^{3+} will be facilitated, resulting in the enhancement of UCL intensity;[33] Second, introducing Yb^{3+} into the framework of $NaErF_4$ host could also induce structural inhomogeneity due to the larger rare earth ion (Er^{3+}) were replaced by smaller rare earth ion (Yb^{3+}), leading to the enhancement for UCL intensity.[44,45]

To reveal the UC mechanism, the excitation power dependent UC emissions of green and red were investigated (Figure 3c and d) as the following formula, $I_{UC} \propto P_{IR}^{n}$.[46,47] Where n is the absorbed photon numbers for each emission and its value can be calculated by the slop of the fitted line of the plot of $\mathrm{Ln}(I_{UC})$ versus $\mathrm{Ln}(P_{IR}^{n})$. As shown in Figure 3d, the slopes of the linear fits for the green at 520 and 545 nm, and red emissions at 664 nm in $NaErF_4$: 30% Yb^{3+} nanorods are 1.44, 1.89, and 1.65, respectively. The results implied that green and red UCL are two photon process.

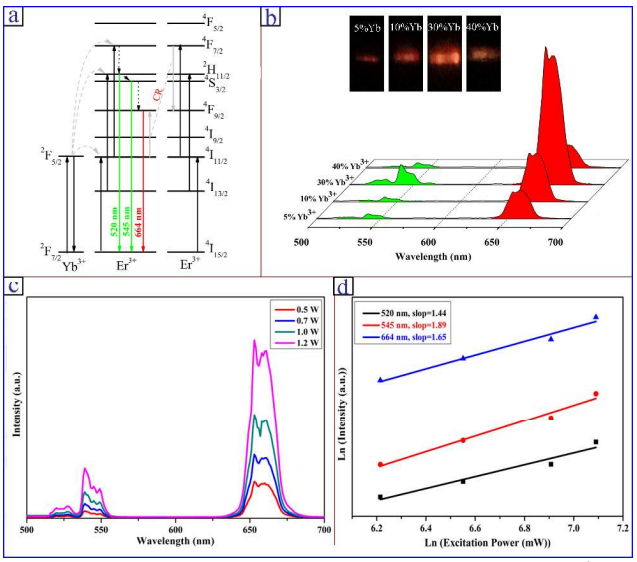

Figure 3. (a) The simple schematic energy-level diagram of Yb^{3+} and Er^{3+}; (b) UC spectra of the $NaErF_4$: X% Yb^{3+} (X= 5, 10, 30, and 40) samples; (c) UC spectra of $NaErF_4$: 30% Yb^{3+} samples under various exciting power (0.5W, 0.7W, 1.0W, and 1.2W); (d) The Ln(*UC intensity*)-Ln(*excitation power*) plots of the UCL intensity versus excitation power. The insets of Figure 3b are the corresponding digital photographs of the $NaErF_4$: X% Yb^{3+} (X= 5, 10, 30, and 40) nanocrystals dispersed in cyclohexane solution.

3.3. *In-vitro* cell fluorescent imaging

To verify the ability of fluorescent bioimaging, the *in vitro* bioimaging of HeLa cells treated with the ligand-free $NaErF_4$: 30% Yb^{3+} nanorods were investigated by a con-focal laser scanning microscope. As shown in Figure 4b, the cells exhibited bright red UC fluorescence, indicating the nanorods were incorporated into HeLa cells efficiently. The overlay image (Figure 4c) shows that the UCL emission was matched well with the HeLa cells. The inset of Figure 4c shows the localized UC spectra taken from HeLa cells and background in the spectral range of 600-700 nm. As demonstrated, strong red UCL can be observed in HeLa cells (red line) without any autofluorescence and large signal-to-noise ratio of 290, further verifying the nanoprobes were successfully grafted onto the HeLa cells. The above results indicate that $NaErF_4$: 30% Yb^{3+} nanorods can be used as ideal nanoprobe for UC fluorescent bioimaging with high contrast and absence of autofluorescence.

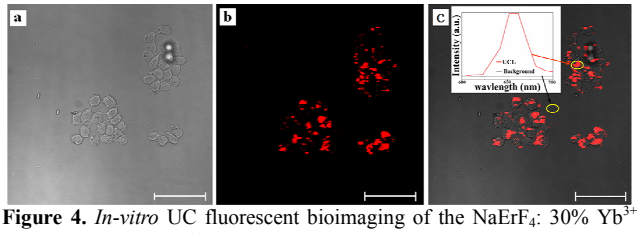

Figure 4. *In-vitro* UC fluorescent bioimaging of the $NaErF_4$: 30% Yb^{3+} nanorods in HeLa cell: (a) bright field image; (b) red UCL image was collected at 600-700 nm; (c) the overlay of UCL image, The insets of (c) show the localized photoluminescence spectra taken from HeLa cells and background in spectral range of 600-700 nm. Scale bars are 100 μm for a-c.

3.4. T_2-weighted MRI

Owing to its exceptional spatial and anatomical resolution, MRI has been widely used in diagnostic imaging over the past decades. According to the previous research, the magnetizations of $NaErF_4$ nanorods (190 ℃, 12h) are measured to 2.53 emu g^{-1} at 20 kOe,[32] which is larger than the previous reported magnetization of the Gd based materials.[36,47,48] However, compared with the commonly used MRI contrast agents containing Gd^{3+}, Er-based contrast agents possess some different properties: (1) shorter electronic relaxation time, (2) relaxing protons via Curie mechanism, (3) larger magnetic moment (9.59 μ_B),[37] which may resulting in efficient T_2 relaxation for MRI. The phantom T_2-weighted MRI for the aqueous solutions containing different concentrations of hydrophilic $NaErF_4$: 30% Yb^{3+} nanorods (0-0.8 mM) were tested under a 4.7 T magnetic resonance system. As shown in Figure 5, the signal was attenuated by gradually increasing the concentrations of $NaErF_4$: 30% Yb^{3+} nanorods. This study has demonstrated that Er-based materials can act as an effective T_2-weighted MRI contrast agent.

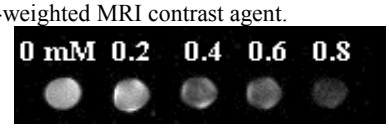

Figure 5. *In vitro* T_2-weighted MRI images of various molar concentrations of hydrophilic $NaErF_4$: 30% Yb^{3+} nanorods (0, 0.2, 0.4, 0.6, and 0.8 mM).

3.5. *In vivo* X-ray imaging

Due to the large K-edge energy (57.49 keV) of Er,[38] the Er-based host materials have promising application in nanoparticle-based X-ray imaging contrast agents. To demonstrate the ability of X-ray imaging, a nude mouse subcutaneously injected with a certain amount aqueous solution of hydrophilic $NaErF_4$: 30% Yb^{3+} (200 μL, 3 mg/mL) was detected at 35 kVp. Compared with the pre-injection image (Figure 6a), an obvious X-ray absorption contrast marked by red circle can be observed after subcutaneous injection (Figure 6b). The results suggest that Er-based materials can be used as X-ray imaging contrast agents and this is the first time for

the *in vivo* X-ray imaging based on the Er-based host.

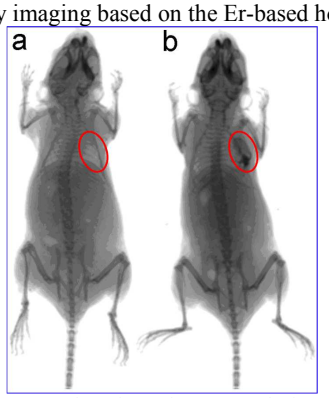

Figure 6. *In vivo* X-ray imaging of a mouse before (a) and after (b) subcutaneous injection 200 μL of hydrophilic $NaErF_4$: 30% Yb^{3+} nanorods.

4. Conclusions

To sum up, various contents of Yb^{3+} doped multi-functional $NaErF_4$ nanorods with high quality were synthesized by a facile hydrothermal method. The UCL intensity of the $NaErF_4$ is increased by doping the sensitizer Yb^{3+} and the strongest UCL intensity can be obtained by doping 30% Yb^{3+}. While, when further increasing the doped Yb^{3+} content to 40%, the UCL intensity is dramatically decreased owing to the formation of small cubic phase nanoparticles (about 15 nm). Moreover, these Er-based materials possess large R/G ratio and dominant red UCL, which is different with previously reported Y-based host with green UCL. The as-prepared hydrophilic $NaErF_4$:Yb UCL nanorods have been successfully used in *in-vitro* cell fluorescent imaging with excellent signal-to-noise ratio. Moreover, the Er-based materials can provide another imaging capacity as MRI probes. Besides, *in vivo* X-ray imaging based on these Er-based materials were demonstrated for the first time, indicating these Er-based materials are ideal contrast agents for X-ray imaging. Therefore, these multi-functional Yb^{3+} doped $NaErF_4$ including dominant red UCL, paramagnetic, and X-ray absorption properties, may have promising applications in biological field for multi-modal MRI/CT/Optical bioimaging, especially in *in vivo* optical bioimaging for deeper tissue penetration.

Acknowledgments

This work was supported by the National Natural Science Foundation of China (Nos. 51102202, and 91230116), specialized research Fund for the Doctoral Program of Higher Education of China (No. 20114301120006) and Hunan Provincial Natural Science Foundation of China (Nos. 12JJ4056 and 13JJ1017), the Scientific Foundation of Ministry of Education (212119) and Scientific Research Fund of Hunan Provincial Education Department (13B062).

Notes and references

[a] *College of Physics and Information Science and Key Laboratory of Low-dimensional Quantum Structures and Quantum Control of the Ministry of Education, Hunan Normal University, Changsha, Hunan, China. Email: songjunz@hunnu.edu.cn*

[b] *Faculty of Materials, Optoelectronics and Physics, Key Laboratory of Low-dimensional Materials and Application Technology (Ministry of Education), Xiangtan University, Xiangtan 411105, People's Republic of China.*

[c] *Department of Applied Physics and Materials Research Center, The Hong Kong Polytechnic University, Hong Kong.*

1. G. Y. Chen, T. Y. Ohulchanskyy, A. Kachynski, H. Agren and P. N. Prasad, *ACS Nano*, 2011, **5**, 4981-4986.
2. N. N. Dong, M. Pedroni, F. Piccinelli, G. Conti, A. Sbarbati, J. E. Ramírez-Hernández, L. M. Maestro, M. C. Iglesias-de la Cruz, F. Sanz-Rodriguez, A. Juarranz, F. Chen, F. Vetrone, J. A. Capobianco, J. G. Solé, M. Bettinelli, D. Jaque and A. Speghini, *ACS Nano*, 2011, **5**, 8665-8671.
3. F. Wang, R. R. Deng, J. Wang, Q. X. Wang, Y. Han, H. M. Zhu, X. Y. Chen and X. G. Liu, *Nat. Mater.*, 2011, **10**, 968-973.
4. D. K. Chatterjee, A. J. Rufaihah and Y. Zhang, *Biomaterials*, 2008, **29**, 937-943.
5. G. Y. Chen, J. Shen, T. Y. Ohulchanskyy, N. J. Patel, A. Kutikov, Z. P. Li, J. Song, R. K. Pandey, H. Agren, P. N. Prasad and G. Han, *ACS Nano*, 2012, **6**, 8280-8287.
6. N. M. Idris, M. K. Gnanasammandhan, J. Zhang, P. C. Ho, R. Mahendran and Y. Zhang, *Nat. Med.*, 2012, **18**, 1580-1585.
7. J. F. Jin, Y. J. Gu, C. W. Y. Man, J. P. Cheng, Z. H. Xu, Y. Zhang, H. S. Wang, V. H. Y. Lee, S. H. Cheng and W. T. Wong, *ACS Nano,* 2011, **5**, 7838-7847.
8. F. Wang, Y. Han, C. S. Lim, Y. H. Lu, J. Wang, J. Xu, H. Y. Chen, C. Zhang, M. H. Hong and X. G. Liu, *Nature*, 2010, **463**, 1061-1065.
9. F. Wang, and X. G. Liu, *J. Am. Chem. Soc.*, 2008, **130**, 5642-5643.
10. J. N. Liu, W. B. Bu, L. M. Pan and J. L. Shi, *Angew. Chem. Int. Ed.*, 2013, **52**, 4375-4379.
11. M. K. G. Jayakumar, N. M. Idris and Y. Zhang, *Proc. Natl. Acad. Sci. USA*, 2012, **109**, 8483-8488.
12. C. Wang, L. Cheng, Y. M. Liu, X. J. Wang, X. X. Ma, Z. Y. Deng, Y. G. Li and Z. Liu, *Adv. Funct. Mater.*, 2013, **23**, 3077-3086.
13. Y. F. Wang, G. Y. Liu, L. D. Sun, J. W. Xiao, J. C. Zhou and C. H. Yan, *ACS Nano*, 2013, **7**, 7200-7206.
14. H. Dong, L. D. Sun and C. H. Yan, *Nanoscale*, 2013, **5**, 5703-5714.
15. C. Wang, L. Cheng and Z. Liu,*Theranostics,* 2013, **3**, 317-330.
16. H. P. Zhou, C. H. Xu, W. Sun and C. H. Yan, *Adv. Funct. Mater.*, 2009, **19**, 3892-3900.
17. F. C. J. M. van Veggel, C. H. Dong, N. J. J. Johnson and J. Pichaandi, *Nanoscale*, 2012, **4**, 7309-7321
18. J. Zhou, Z. Liu and F. Y. Li, *Chem. Soc. Rev.*, 2012, **41**, 1323-1349.
19. Q. F. Xiao, X. P. Zheng, W. B. Bu, W. Q. Ge, S. J. Zhang, F. Chen, H. Y. Xing, Q. G. Ren, W. P. Fan, K. L. Zhao, Y. Q. Hua and J. L. Shi, *J. Am. Chem. Soc.*, 2013, **135**, 13041-13048.
20. S. J. Zeng, J. J. Xiao, Q. B. Yang, and J. H. Hao, *J. Mater. Chem.*, 2012, **22**, 9870-9874.
21. P. A. Ma, H. H. Xiao, X. X. Li, C. X. Li, Y. L. Dai, Z. Y. Cheng, X. B. Jing and J. Lin, *Adv. Mater.*, 2013, **25**, 4898-4905.
22. D. M. Yang, X. J. Kang, P. A. Ma, Y. L. Dai, Z. Y. Hou, Z. Y. Cheng, C. X. Li and J. Lin, *Biomaterials*, 2013, **34**, 1601-1612.
23. M. Haase and H. Schäfer, *Angew. Chem. Int. Ed.*, 2011, **50**, 5808-5829.
24. H. Schäfer, P. Ptacek, K. Kömpe and M. Haase, *Chem. Mater.*, 2007, **19**, 1396-1400.
25. C. X. Li, J. Yang, Z. W. Quan, P. P. Yang, D. Y. Kong and J. Lin, *Chem. Mater.*, 2007, **19**, 4933-4942.
26. C. X. Li, D. M. Yang, P. A. Ma, Y. Y. Chen, Y. Wu, Z. Y. Hou, Y. L. Dai, J. H. Zhao, C. P. Sui and J. Lin, *Small*, 2013, DOI: 10.1002/smll.201301093.
27. S. J. Zeng, H. B. Wang, W. Lu, Z. G. Yi, L. Rao, H. R. Liu and J. H. Hao, *Biomaterials,* 2013, DOI:10.1016/j.biomaterials.2013.11.082.
28. Y. L. Dai, P. A. Ma, Z. Y. Cheng, X. J. Kang, X. Zhang, Z. Y. Hou, C. X. Li, D. M. Yang, X. F. Zhai and J. Lin, *ACS Nano*, 2012, **6**, 3327-3338.
29. C. X. Li and J. Lin, *J. Mater. Chem.*, 2010, **20**, 6831-6847.
30. Y. L. Dai, H. H. Xiao, J. H. Liu, Q. H. Yuan, P. A. Ma, D. M. Yang, C. X. Li, Z. Y. Cheng, Z. Y. Hou, P. P. Yang and J. Lin, *J. Am. Chem. Soc.*, 2013, DOI**:** 10.1021/ja410028q.

31. K. W. Krämer, D. Biner, G. Frei, H. U. Güdel, M. P. Hehlen and S. R. Lüthi, *Chem. Mater.*, 2004, **16**, 1244-1251.
32. H. B. Wang, Z. G. Yi, L. Rao, H. R. Liu and S. J. Zeng, *J. Mater. Chem. C*, 2013, **1**, 5520-5526.
33. N. Niu, P. P. Yang, F. He, X. Zhang, S. L. Gai, C. X. Li and J. Lin, *J. Mater. Chem.*, 2012, **22**, 10889-10899.
34. J. Zhou, M. X. Yu, Y. Sun, X. Z. Zhang, X. J. Zhu, Z. H. Wu, D. M. Wu, and F. Y. Li, *Biomaterials*, 2011, **32**, 1148-1156.
35. H. Y. Xing, W. B. Bu, S. J. Zhang, X. P. Zheng, M. Li, F. Chen, Q. J. He, L. P. Zhou, W. J. Peng, Y. Q. Hua, and J. L. Shi, *Biomaterials*, 2012, **33**, 1079-1089.
36. S. J. Zeng, M. K. Tsang, C. F. Chan, K. L. Wong, and J. H. Hao, *Biomaterials*, 2012, **33**, 9232-9238.
37. S. Viswanathan, Z. Kovacs, K. N. Green, S. J. Ratnakar and A. D. Sherry, *Chem. Rev.*, 2010, **110**, 2960-3018.
38. http://physics.nist.gov/PhysRefData/XrayMassCoef/.
39. S. B. Yu and A. D. Watson, *Chem. Rev.*, 1999, **99**, 2353-2378.
40. X. Wang, J. Zhuang, Q. Peng and Y. D. Li, *Nature*, 2005, **437**, 121-124.
41. S. J. Zeng, G. Z. Ren, C. F. Xu and Q. B. Yang, *CrystEngComm*, 2011, **13**, 1384-1390.
42 N. Bogdan, F. Vetrone, G. A. Ozin, and J. A. Capobianco, *Nano Lett.*, 2011, **11**, 835-840.
43. R. D. Shannon, *Acta Cryst.*, 1976, **32**, 751–767.
44. X. Teng, Y. H. Zhu, W. Wei, S. C. Wang, J. F. Huang, R. Naccache, A. Tok, Y. Han, Q. C. Zhang, J. A. Capobianco and L. Huang, *J. Am. Chem. Soc.*, 2012, **134**, 8340-8343.
45. V. S. Mironov, *Spectrochim. Acta, Part A*, 1998, **54**, 1607-1614.
46. F. Vetrone, J. C. Boyer, J. A. Capobianco, A. Speghini and M. Bettinelli, *J. Appl. Phys.*, 2004, **96**, 661-667.
47. G. Z. Ren, S. J. Zeng, and J. H. Hao, *J. Phys. Chem. C*, 2011, **115**, 20141-20147.
48. H. T. Wong, F. Vetrone, R. Naccache, H. L. W. Chan, J. H. Hao and J. A. Capobianco, *J. Mater. Chem.*, 2011, **21**, 16589-16596.

Multi-functional $NaErF_4$:Yb nanorods: enhanced red upconversion emission, *in vitro* cell, *in vivo* X-ray, and T_2-weighted magnetic resonance imaging

Haibo Wang,[a,b] Wei Lu,[c] Tianmei Zeng,[a] Zhigao Yi, [a,b] Ling Rao, [a,b] Hongrong Li [a] and Songjun Zeng[*a]

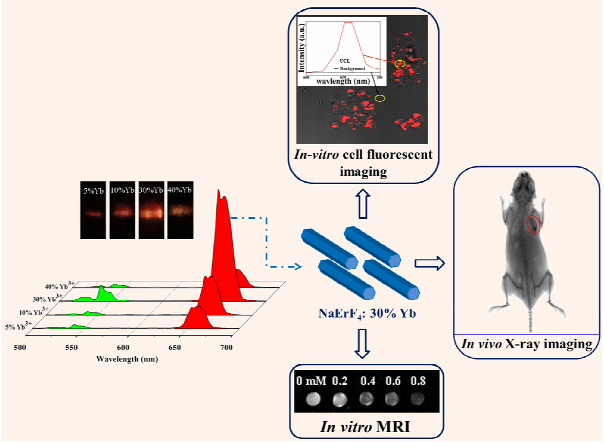

A new type of multi-functional $NaErF_4$ nanoprobe with enhanced red upconversion emission was developed and used for *in vitro* cell, *in vivo* X-ray and T_2-weighted magnetic resonance imaging for the first time.